

# Bioinspired Surface for Surgical Graspers Based on the Strong Wet Friction of Tree Frog Toe Pads

Huawei Chen,<sup>\*,†</sup> Liwen Zhang,<sup>†</sup> Deyuan Zhang,<sup>\*,†</sup> Pengfei Zhang,<sup>†</sup> and Zhiwu Han<sup>‡</sup>

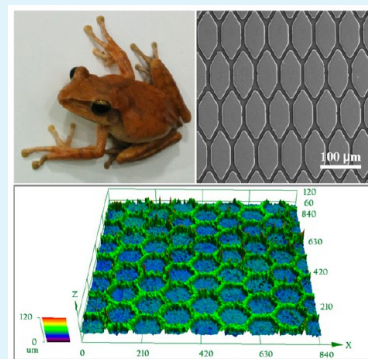
<sup>†</sup>School of Mechanical Engineering and Automation, Beihang University, No. 37 Xueyuan Road, Haidian District, Beijing, 100191, China

<sup>‡</sup>Key Laboratory for Bionic Engineering, Ministry of Education, Jilin University, Changchun 130022, China

## S Supporting Information

**ABSTRACT:** Soft tissue damage is often at risk during the use of a surgical grasper, because of the strong holding force required to prevent slipping of the soft tissue in wet surgical environments. Improvement of wet friction properties at the interface between the surgical grasper and soft tissue can greatly reduce the holding force required and, thus, the soft tissue damage. To design and fabricate a biomimetic microscale surface with strong wet friction, the wet attachment mechanism of tree frog toe pads was investigated by observing their epithelial cell structure and the directionally dependent friction on their toe pads. Using these observations as inspiration, novel surface micropatterns were proposed for the surface of surgical graspers. The wet friction of biomimetic surfaces with various types of polygon pillar patterns involving quadrangular pillars, triangular pillars, rhomboid pillars, and varied hexagonal pillars were tested. The hexagonal pillar pattern exhibited improved wet frictional performance over the modern surgical grasper jaw pattern, which has conventional macroscale teeth. Moreover, the deformation of soft tissue in the bioinspired surgical grasper with a hexagonal pillar pattern is decreased, compared with the conventional surgical grasper.

**KEYWORDS:** wet friction, tree frog, biomimetic surface, surgical grasper, low damage



## 1. INTRODUCTION

A surgical grasper is used to grasp the soft tissue and organs during surgical operations; it is one of the most popular surgical instruments. However, the use of a grasper is risky, because of the possibility of exerting an undesirable overloading force to avoid soft tissue slippage, and many grasper-related traumas have occurred during laparoscopic procedures.<sup>1–8</sup> During laparoscopic surgeries, 25% of gall bladder perforations are caused by grasper trauma,<sup>1</sup> and bowel perforation caused by laparoscopic instruments can increase morbidity and mortality rates to 20%.<sup>9,10</sup> Several novel approaches have been proposed to address this problem, such as integrating pressure sensors<sup>11,12</sup> into the graspers or replacing the conventional grasper with a vacuum grasper.<sup>13</sup> Unfortunately, soft tissue damage cannot be avoided in the sensor-integrated instrument, because of the nonuniform pressure distribution, and the vacuum grasper has difficulty manipulating any small or irregular parts, such as blood vessels. Optimization of grasper jaw design is still the most commonly used approach to decrease soft tissue damage. Strong grasping with low damage or even no damage to soft tissue is the ideal functionality of the surgical grasper.

For strong grasping, animals and insects have evolved many marvelous grasping strategies to freely move in their living environments. Generally, the many varied strategies can be categorized into two types, i.e., sharp claws and attachable toe pads. The teeth on the conventional surgical grasper jaw

resemble the sharp claw and cannot balance grip security and tissue damage.<sup>14</sup> Although an optimal jaw design can reduce soft tissue damage,<sup>15</sup> the macroscale teeth of the jaw induce stress that inevitably results in damage of the soft tissue, because of the overloading grasping force usually exerted to avoid any sliding. Any surgical grasper with macroscale teeth functions by embedding teeth into soft tissue. Another natural grasping method is based on the adhesion and friction of creatures' soft pads, including the hairy attachment systems used by geckos and the smooth attachment systems found in tree frogs. The contact force of hairy attachment systems is greatly reduced in a wet environment,<sup>16,17</sup> whereas smooth attachment systems constructed with pillar arrays could maintain considerable frictional force on wet surfaces.<sup>18</sup> Tree frogs, as animals with smooth attachment systems, can vertically climb trees in wet environments because of their strong wet attachment ability. Because the surgical environment is filled with bodily fluids similar to the living environment of the tree frog, the strategies of the tree frog for wet attachment can inspire the design of novel surgical graspers to minimize damage to soft tissue.

Many studies demonstrate that the toe pad of the tree frog is constructed with tightly arrayed epithelial cells, most of which

Received: April 8, 2015

Accepted: June 8, 2015

Published: June 8, 2015

are irregular polygons, and covered with a layer of mucus.<sup>19–22</sup> Endlein et al. discovered that the torrent frog possesses a stronger frictional force on wet surfaces than the tree frog and speculated that the orientation of channels on its toe pad may influence frictional force.<sup>23</sup> Using the tree frog as inspiration, many novel biomimetic surfaces have been proposed recently. For example, Shahsavan et al. fabricated adhesive materials with base micropillars that can create significant adhesion.<sup>24</sup> Roshan et al. used a tree frog-inspired material in an intra-abdominal device to fix the smooth and wet peritoneum during minimally invasive surgery.<sup>25</sup> However, nearly all of these studies focused solely on the feasibility of a biomimetic regular hexagon pillar pattern, and the mechanisms of wet attachment, especially the effect of surface micropattern, are still unclear. Moreover, no studies have been published about bioinspired applications in minimally invasive surgical devices.

In this paper, the microscale structure characteristics of the tree frog toe pad were observed by scanning electron microscopy (SEM), and its structure features were investigated. In particular, the effect of micropatterns on wet friction was explored by changing the sliding direction of the tree frog toe pad and the shape of the micropattern. Micropatterns with hexagonal pillars, rhomboid pillars, triangular pillars, and quadrangular pillars were proposed to investigate their wet friction performance via comparison with the modern surgical grasper jaw. Using the inspiration of the irregular hexagonal cells on the tree frog toe pads, we designed a varied hexagonal pillar pattern with different types of top corner angles and investigated the variation in their wet friction along different sliding directions. Finally, the soft tissue damage of these patterns was evaluated, and the effectiveness of biomimetic surface patterns when applied in surgical graspers was confirmed.

## 2. MATERIAL AND METHODS

**2.1. Preparation of the Natural Specimen and Biomimetic Surface Structure.** Mature spotted-leg tree frogs (*Polypedates megacephalus*, family Hylidae) were used as the biological prototype. Their toe specimens were rapidly prepared with an SEM specimen fix procedure, which included cleaning, fixing, dehydrating, and vacuum drying. To obtain comparable surface patterns, all surface patterns were fabricated in polydimethylsiloxane (PDMS, Dow Corning, Sylgard 184) blocks (10 mm × 10 mm in area, 8 mm high) with an elastomer:cross-linker ratio of 10:1. Macroscale teeth patterns of the modern surgical grasper were duplicated from laser-cut aluminum teeth patterns. Pillar patterns were replicated from microstructured templates that were fabricated using the SU-8 photolithography technique.<sup>26</sup>

**2.2. Measurement of the Wet Friction Force.** A two-dimensional (2D) force transducer and an XYZ-translation stage (Siskiyou, Inc., 7600 Series) were used as the force measuring equipment. Testing samples were fixed and moved by the translation stage (Figure 1). The recordable maximum normal force and friction force were 10 000 mN, and the noise was <0.1 mN. To measure the friction of the tree frog, the body of the tree frog was confined in a box with its legs protruding outside. The toe pad was immobilized with a tube connected to a vacuum pump (Figure 1b). The normal force and sliding speed were maintained at 3 mN and 300  $\mu\text{m/s}$ , respectively. After each sliding, the toe pad had a 3 min resting period for secretion recovery. The frictional force was measured 20 times in both the proximal and lateral directions. To measure the

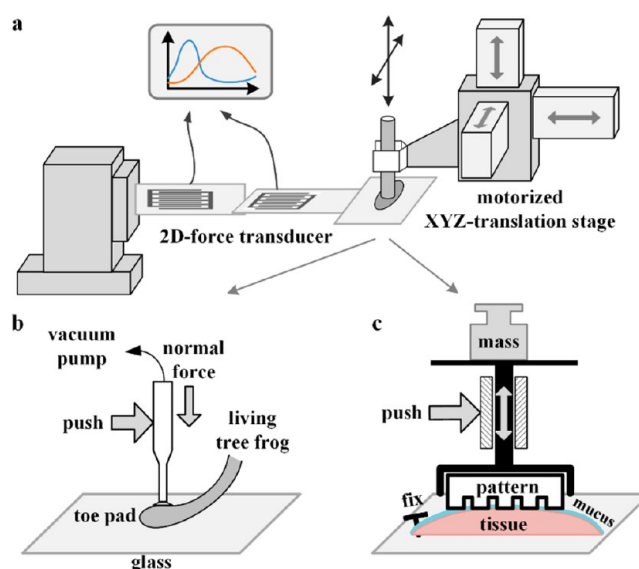


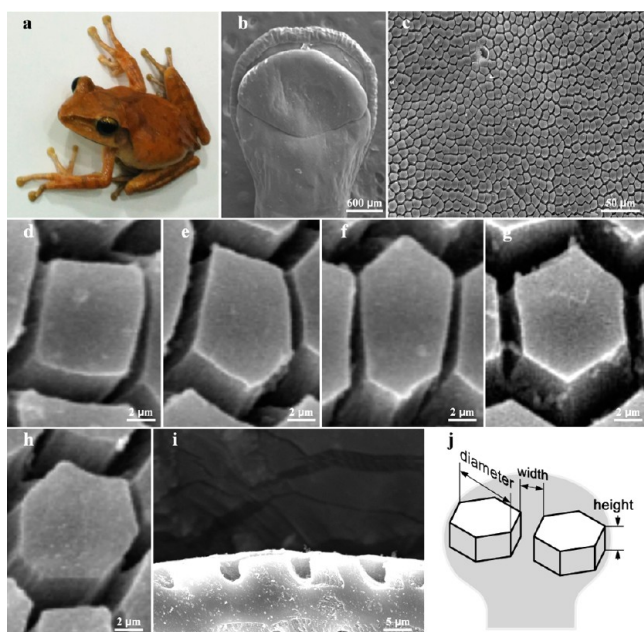
**Figure 1.** (a) Structural schematic of the friction force measuring equipment. (b) Measurement method for the tree frog's toe pad. (c) Measurement method for the biomimetic surface.

friction of the surface patterns, the PDMS blocks were mounted onto a piece of metal sheet and moved by the translation stage. A piece of fresh pig liver tissue was fixed to the substrate (Figure 1c). A weight of 5000 mN was fixed to the metal sheet to create a constant pressure of 50 kPa, which is less than the failure pressure of fresh pig liver (160–280 kPa).<sup>27</sup> The sliding speed was set to 500  $\mu\text{m/s}$ . Prior to the friction test, 0.5 mL of deionized water was injected onto the tissue surface to imitate the wet environment inside the human body, then the PDMS block was pressed onto it. The frictional force of each pattern was separately measured 10 times in both the horizontal and vertical directions.

**2.3. Microscopic Observation.** An SEM system (Model JSM-6010LA, JEOL, Ltd.) was used to observe the surface morphology. An inverted biological microscope (Chongqing Optical & Electrical Instrument Co., Ltd.) was used to observe the movement of liquid upon the interface between the biomimetic surface pattern and a glass slide. The surface pattern was fixed, and the sliding speed of the glass slide was controlled to  $\sim 500 \mu\text{m/s}$ . Approximately 0.5 mL of deionized water mixed with Chinese ink was filled onto the glass slide for imaging purposes before the PDMS block pressed onto it. Surface-pattern-caused tissue deformation was measured using a laser confocal microscope (Model OLS4100, Olympus Co.). The tissue was first pinched by the surface pattern and then frozen in liquid nitrogen to fix the deformation prior to observation.

## 3. RESULTS AND DISCUSSION





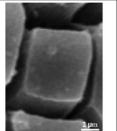
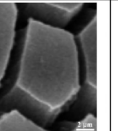
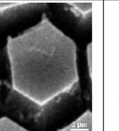
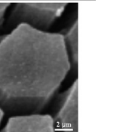
**3.1. Structural Characteristics of the Toe Pad and Its Direction-Dependent Friction.** The tree frog species *Polypedates megacephalus* has strong climbing skills, because of its attachable toe pads (Figure 2a). The toe pads are constructed with tightly arrayed epithelial cells and formed connected channels. The width of the channels, the circumference diameter, and the height of the epithelial cells are  $\sim 1$ , 10, and 5  $\mu\text{m}$ , respectively, on average. An illustrated schematic is shown in Figure 2j. Most cells are hexagonal pillars, accounting for  $\sim 55\%$  of epithelial cells, whereas the remaining cells are pentagonal, heptagonal, and quadrangular (see Figures 2d–h,



**Figure 2.** (a) Spotted-leg tree frog, *Polypedates megacephalus* (snout–vent length, ~50 mm). (b) Low-power SEM image of an entire tree frog toe pad. (c) High-power SEM image of epithelial cells. (d–h) Quadrangular epithelial cell, pentagonal epithelial cell, irregular hexagonal epithelial cell, regular hexagonal epithelial cell, and heptagonal epithelial cell, respectively. (i) Sectional view of toe pad. (j) Schematic of epithelial cells.

as well as Table 1). Moreover, although there exist regular hexagonal pillars, the hexagonal pillars are mainly irregular.

**Table 1. Characteristics of Epithelial Cells from Tree Frog Toe Pads<sup>a</sup>**

The type of micro-pattern of epithelial cell				
	quadrangle	pentagon	hexagon	heptagon
SEM image				
Proportion (%)	1	26	55	18

<sup>a</sup>A total of 1455 epithelial cells from 3 toe pads were counted.

To elucidate the effect of the irregular polygon epithelial cells, the frictional force of tree frog toe pads was measured in two sliding directions. The proximal direction (P) was defined as the extruding direction of the toe pads, and the lateral direction (L) was defined as the direction perpendicular to proximal, as shown in Figure 3. The friction of the tree frog's toe pad in proximal slides is ~20% higher than in lateral slides. As demonstrated by Seo et al., the gecko's spatula-inspired micropillars also have similar anisotropic adhesion, because of their unique structure.<sup>28</sup> The specific friction-direction-dependent features of the tree frog's toe pads could result from their anisotropic microstructure, leading to directional dependence in friction, because of the different flow conditions of liquid in the channels.

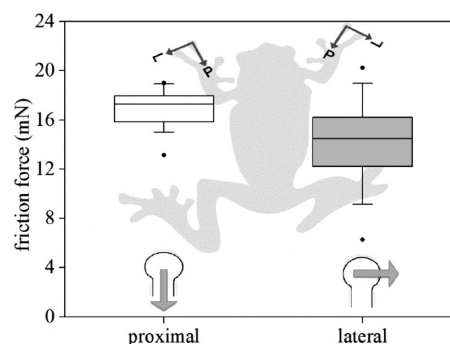


**Figure 3.** Frictional force in different sliding directions (proximal vs lateral) of a tree frog's toe pad. P and L denote proximal and lateral directions, respectively.

The distribution of channels was analyzed by collecting data from 2483 lines in three SEM image (see Figures 4a and 4b) and the angle  $\theta$  formed by the channel and the proximal direction of the toe pads. According to  $\theta$ , all lines were distributed into 9 sections, from  $0^\circ$  to  $90^\circ$ . In each section, the number of lines was counted, and their lengths were summarized. The channels' distribution slowly decreases as the angle  $\theta$  increases from  $0^\circ$  to  $90^\circ$  (Figure 4a). Channels ranging from  $0^\circ$  to  $10^\circ$  appear twice as often as channels ranging from  $80^\circ$  to  $90^\circ$ . This shows that these channels predominantly align along the climbing direction of the tree frog, which is the proximal direction of the toe pad. Since the channel's length also has a great impact on the secretion flow, the lengths are summarized for each section, as shown in Figure 4b. The length tendencies are similar to those of the channel orientation, but the change is more apparent. The summation of channel length in the range of  $0^\circ$ – $10^\circ$  is ~4 times greater than the length ranging from  $80^\circ$  to  $90^\circ$ , indicating that the channel will be longer if it is oriented more closely to the proximal direction.

Because the epithelial cells were mainly hexagonal, the aspect ratio, defined as the ratio of cell projection on proximal  $a$  to that on lateral  $b$  of the toe pad, of 814 hexagonal epithelial cells was collected (see Figure 4c). The mean value of the aspect ratio of hexagonal epithelial cells was ~1.46. Compared with the highest aspect ratio of a regular hexagonal polygon (1.15), ~82% of the hexagonal epithelial cells on the toe pads were slimmer than a regular hexagon. This shows that hexagonal epithelial cells on toe pads are irregular and tend to elongate in the proximal direction. This statistical study of tree frog toe pads implies that channels on toe pads have a tendency to orient in the proximal direction, and the epithelial cells are irregular and slim in the proximal direction. These structural characteristics may have a strong impact on the flow of secretion, affecting the tree frog's climbing ability.

**3.2. Effect of the Surface Pattern on the Wet Friction Force.** **3.2.1. Friction Measurement of Different Polygon Surface Patterns.** The jaws on a modern surgical grasper are constructed with sharp teeth arrays (Figure 5). During grasping, the tissue deforms and fills the gaps between the teeth arrays to achieve a secure grip. Significant deformation occurs and leads to stress concentration of soft tissue, and thus, tissue damage is inevitable when using the modern surgical grasper. Based on the variety of modern surgical graspers, we chose two typical types of teeth arrays, i.e., 1 and 0.5 mm macroscale teeth patterns with top corners of  $60^\circ$  and fabricated them on  $10\text{ mm} \times 10\text{ mm}$  PDMS blocks (see Figures 5b and 5c).

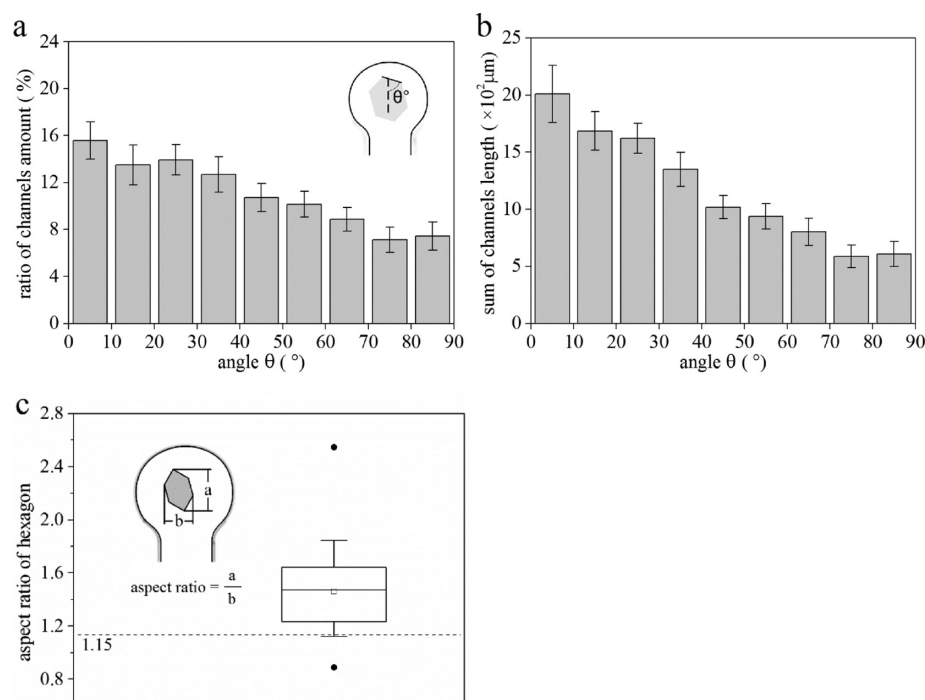


**Figure 4.** Statistics of epithelial cell properties in tree frog toe pads. (a) The ratio of channel quantities at different angles  $\theta$  (angle  $\theta$  was formed by the channel and the direction toward the tree frog's body; data have been collected from 2483 channels). (b) The total length of channels in each section. (c) The aspect ratio of 436 hexagonal epithelial cells from tree frog toe pads have been collected. (The bottom and top of the box are the 25th and 75th percentiles, respectively, and the whiskers represent the 10th and 90th percentiles. Dark dots show the maximum and minimum values. The cube in the box shows that the average aspect ratio of a measured hexagon is 1.46, which is greater than 1.15, the highest aspect ratio of a regular hexagon.)

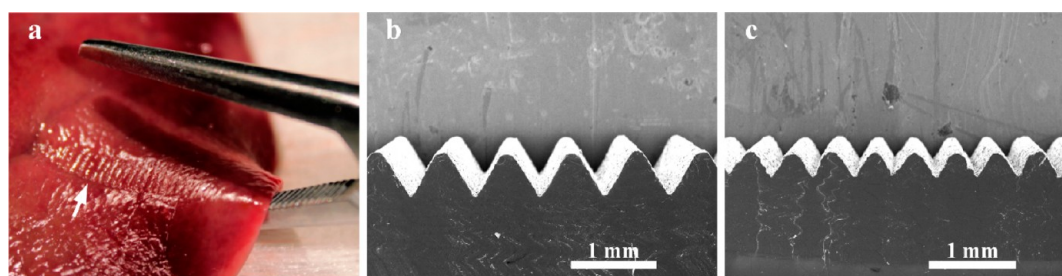


**Figure 5.** (a) Surgical grasper grips a piece of fresh pig liver. Arrow shows the trail left by macroscale teeth. (b, c) SEM images of 1 mm (panel b) and 0.5 mm (panel c) macroscale teeth arrayed on a PDMS block.

**Table 2. Structural Parameters of Various Surface Patterns on a Surgical Grasper**

No.	Surface pattern	Description	Horizontal sliding	Vertical sliding	Tooth width		Tooth angle		
A		1 mm tooth	→	↓	1 mm		60°		
B		0.5 mm tooth			0.5 mm		60°		
C1		Hexagonal pillar			69 $\mu\text{m}$	20 $\mu\text{m}$	30 $\mu\text{m}$	73%	
D		Rhomboid pillar							
E		Triangular pillar							
F		Quadrangular pillar							
R		Smooth surface	$R_a = 0.06 \mu\text{m}$						

Because diamond-shaped teeth with a diameter of 0.15 mm on grasper jaws exhibit significant grasping properties,<sup>15</sup> the

hexagon for the hexagonal pillar pattern is designed with a circumcircle diameter of 140  $\mu\text{m}$ , a side length of 69  $\mu\text{m}$ , a

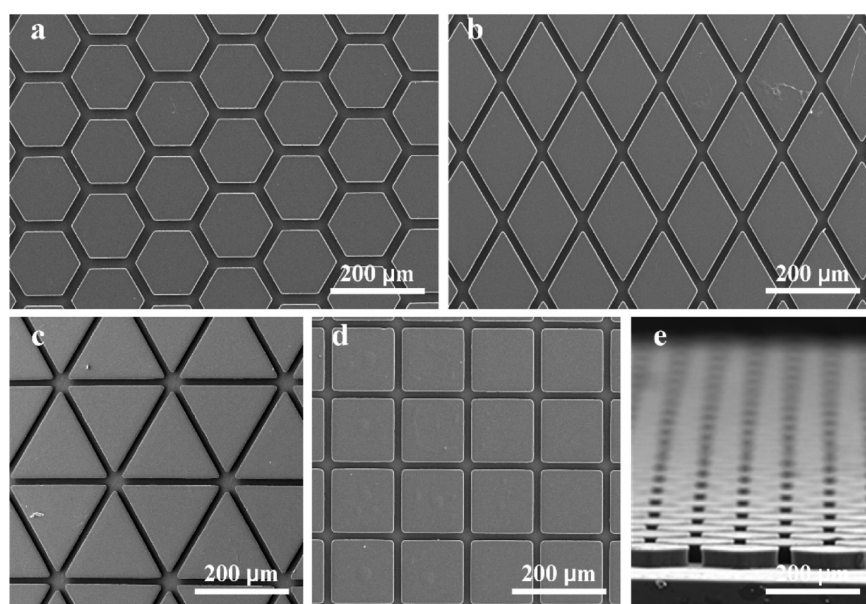


**Figure 6.** SEM images of four different types of polygon pillars: (a) hexagonal pillar, (b) rhomboid pillar, (c) triangular pillar, and (d) quadrangular pillar. Panel e shows a tilted view of pillars with a pillar height of  $\sim 30 \mu\text{m}$ .

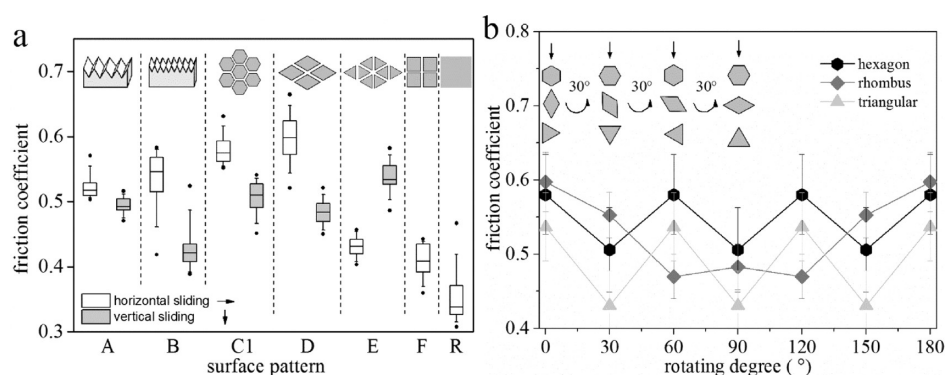


**Figure 7.** (a) Friction coefficient of seven different surface patterns (Table 2) in horizontal and vertical sliding directions. Quadrangular pillar and smooth pattern have the same friction coefficient in both directions. (b) Friction coefficient of the hexagonal pillar, rhomboid pillar and triangular pillar surface patterns when the surface patterns are rotated  $30^\circ$ ,  $60^\circ$ ,  $90^\circ$ ,  $120^\circ$ ,  $150^\circ$  and  $180^\circ$  counterclockwise.

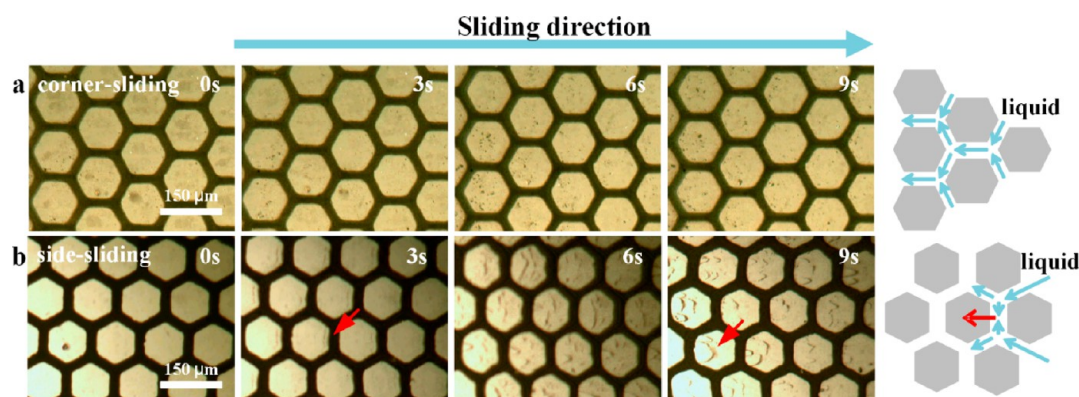


**Figure 8.** Hexagonal pillar surface slid on a glass slide with liquid filled in the contact area. Initial sliding speed was  $0 \text{ mm/s}$ ; results were recorded at times of 0, 3, 6, and 9 s. Dark areas in the pictures indicate liquid mixed with Chinese ink (see the Supporting Information). (a) Surface slid with the hexagon corner toward the sliding direction; black parts are ink in channels. (b) Surface slid with the hexagon side toward the sliding direction. Red arrows indicate the liquid flow on the top of the hexagon pillars. Schematics show the water flowing states.

channel width of  $20 \mu\text{m}$ , and a channel depth of  $30 \mu\text{m}$ . To achieve comparable statistics of friction, pillar patterns with rhombi, triangles and quadrangles were designed with the same

channel depth, channel width, and ratio of contact area (ratio of the pillar top surface to the sum of pillar top surface and channel area) (Table 2). As shown in Figure 6, polygon pillar

patterns were fabricated flawlessly with smooth surfaces, distinct corners, and vertical walls.

Frictional force tests were performed in two sliding directions on tissue—horizontal sliding and vertical sliding—as shown in Table 2. In Figure 7a, all patterns show different friction values, and the majority of them have direction-dependent features. The 0.5 mm macroscale teeth pattern demonstrates stronger friction than the 1 mm teeth pattern in horizontal sliding, whereas the opposite trend appears in vertical sliding. For the polygon pillar patterns, both hexagonal and rhomboid pillar patterns show stronger frictional force than teeth patterns in horizontal and vertical sliding. The friction of triangular and quadrangular pillar patterns is similar to the teeth patterns. By draining liquid on the tissue into channels, these polygon pillar patterns perform considerable frictional force. This indicates that microfriction can enhance frictional force on tissue, compared to the classical teeth–tissue interlock approach.



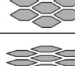

To further investigate the effect of sliding direction on wet friction, hexagonal, rhomboid and triangular pillar patterns were tested at different degrees of rotation (Figure 7b). The structure periods of hexagonal, triangular, and rhomboid pillars are  $60^\circ$ ,  $60^\circ$ , and  $180^\circ$ , respectively; thus, their wet friction also exhibits periodicity with rotation. The variation in wet friction on hexagonal pillars is not as acute, and their friction is increased in all directions, compared with rhomboid and triangular pillars. Thus, 55% hexagonal epithelial cells on tree frog toe pads can generate stable and sufficient frictional force for climbing.

Liquid movement was observed to explore the influence of channels on fluid. When sliding with a hexagon corner forward (hereafter termed “corner sliding”), liquid flowed through channels without apparent flushing onto the contact areas (see Figure 8a, as well as Video S1 in the Supporting Information). However, when setting the hexagon side forward (hereafter termed “side sliding”), some liquid was squeezed onto the contact areas, leaving dark trails (see Figure 8b, as well as Video S2 in the Supporting Information). The liquid flow in corner sliding consisted of the flowing of two-way liquids through the tilt channels, meeting at the angle of the hexagon, flowing along a horizontal channel, and then splitting into two symmetrical tilt channels at the corner (see the schematic in Figure 8a). However, in side sliding, the liquid flowed through a tilt channel and split into two different channels, i.e., a tilt channel and vertical channel. Because of the horizontal sliding of the substrate, the liquid had a tendency to move in the horizontal direction; thus, liquid in vertical channels, such as stagnant water, could only be squeezed out and flushed onto the top of the hexagonal pillars (see the schematic in Figure 8b). This phenomenon can reduce friction, as the liquid can work as a lubricant, and induces the friction direction dependence of the hexagonal pillar pattern. The surface pattern is more slippery if more water remains on the contact area. As a result, the angle formed by channels and the sliding direction has a negative correlation with frictional force. This result may explain why channels on tree frog toe pads have a directional preference. The frictional force in the proximal direction will be stronger (Figure 3) with more channels oriented in the proximal direction on tree frog toe pads (see Figures 4a and 4b), which is suitable for the tree frog’s living environment.<sup>23</sup> Interestingly, this channel effect mechanism may also explain the friction difference between hexagonal, rhomboid, and triangular pillar patterns. As shown in Table 2, the triangular pillar can be

regarded as a rhomboid pillar with an additional vertical channel in the middle. Because of the influence of the vertical channel, the friction coefficient of the triangular pillar surface in vertical sliding is higher than that of the rhomboid pillar, and the opposite trend is observed in the horizontal sliding direction. In another case, the rhomboid pillar can be regarded as a hexagonal pillar with two face-to-face parallel channels removed and the remaining channels connected. This increases the friction coefficient of the hexagonal pillar pattern in horizontal sliding, causing it to be greater than that of the rhomboid pillar pattern in vertical sliding.

**3.2.2. Friction Measurement of Hexagonal Surface Patterns with Different Aspect Ratios.** To explore the influence of different aspect ratios on friction during sliding on tissue, we designed varied hexagonal pillar patterns with top corner angles of  $90^\circ$  (C2),  $60^\circ$  (C3), and  $30^\circ$  (C4), for comparison with the regular hexagonal pillar C1 (see Table 3).

**Table 3. Properties of Four Hexagonal Surface Patterns with Different Top Corner Angles**

No.	Surface pattern	Top corner angle	Side length	Channel width	Channel depth	Contact area	Aspect ratio in corner-sliding
C1		$120^\circ$	69 $\mu\text{m}$	20 $\mu\text{m}$	30 $\mu\text{m}$	73%	1.15
C2		$90^\circ$				69%	1.71
C3		$60^\circ$				56%	2.73
C4		$30^\circ$				37%	5.68

Because the side length of the hexagonal pillar pattern may affect its friction, as noted above, four types of pillars were designed with equal side lengths, channel widths, and channel depths for comparison. These pillar arrays were fabricated flawlessly, as shown in Figure 9.

The friction of four types of hexagonal pillars in corner sliding and side sliding is different and exhibits direction dependence, as shown in Figure 10. The friction coefficient in corner sliding is higher than that observed in side sliding. Even for regular hexagonal pillar C1, its friction coefficient in corner

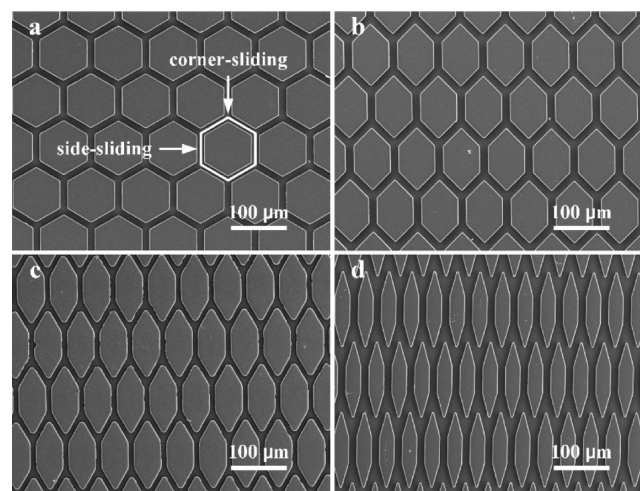


**Figure 9.** SEM images of four different types of hexagonal pillars with top corners of (a)  $120^\circ$ , (b)  $90^\circ$ , (c)  $60^\circ$ , and (d)  $30^\circ$ . Annotation in panel a shows the two sliding directions for the friction test.

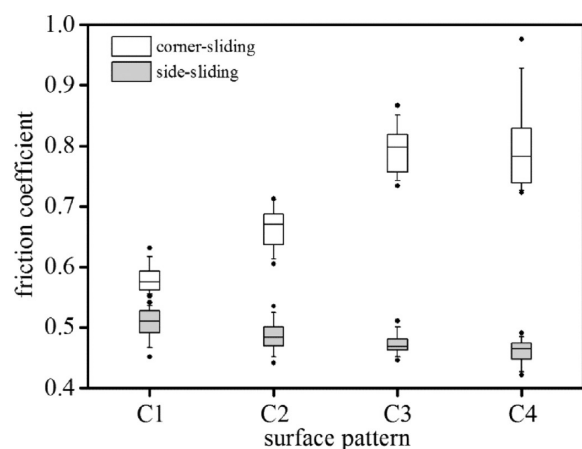


**Figure 10.** Friction coefficient of four types of surface hexagonal patterns with different top corner angles (Table 3) tested in corner sliding and side sliding.

sliding is  $\sim 20\%$  higher than that observed in side sliding. With the hexagonal top corner decreasing, pillars become slimmer and the direction dependence becomes more distinct. For C4 with a top corner of  $30^\circ$ , its friction coefficient in corner sliding is  $\sim 78\%$  higher than in side sliding. Particularly, the change in the effect of the top corner angle on friction in corner sliding is more significant than that in side sliding. From pillar C1 to pillar C4, the friction coefficient in corner sliding increases by  $\sim 34\%$  but only decreases by  $10\%$  over the same range in side sliding. With similar contact and noncontact areas, pillar C3 shows a high friction in corner sliding; this is in agreement with the model in Varenberg's work.<sup>29</sup>

With a smaller top corner angle in corner sliding, the channels orient closer to the corner direction, and a higher frictional force is achieved. The aspect ratio of hexagonal epithelial cells on tree frogs is  $\sim 1.47$  on average, with the top corner angle equal to  $79^\circ$ . When the top corner angle becomes smaller, the wet friction in corner sliding becomes larger. However, the wet friction in side sliding declines as the top corner angle decreases. Moreover, the micropattern may lose stability to bend or deform when the material of the micropattern is not sufficiently hard. The aspect ratio of hexagonal epithelial cells on the toe pad of the tree frog ranges from 0.5 to 2.5. Since the friction measurements were performed on soft tissues with water, the direction-dependent friction is more likely to be induced by flowing of water, which is quite different from Iturri's work.<sup>30</sup> The elasticity of the material and the aspect ratio of the hexagonal pillars must be properly matched to achieve sufficient friction.

### 3.3. Deformation of Soft Tissue Induced by the Biomimetic Surface Pattern for a Surgical Grasper.

According to the studies above, the hexagonal pillar pattern exhibits sufficient wet friction performance in all directions, compared to macroscale teeth patterns and other types of polygon pillar patterns, and slim hexagonal pillar patterns generate considerably more friction, compared to regular hexagonal pillars.

The original macroscale teeth pattern used in surgical graspers inevitably leads to nonuniform deformation, and larger macroscale teeth produce larger tissue deformation (see Figures 11a and 11b). Thus, the stress concentration upon soft tissue cannot be prevented. However, because channels in the hexagonal pillar pattern are narrow and shallow, tissue deformation will be considerably smaller (Figure 11c),

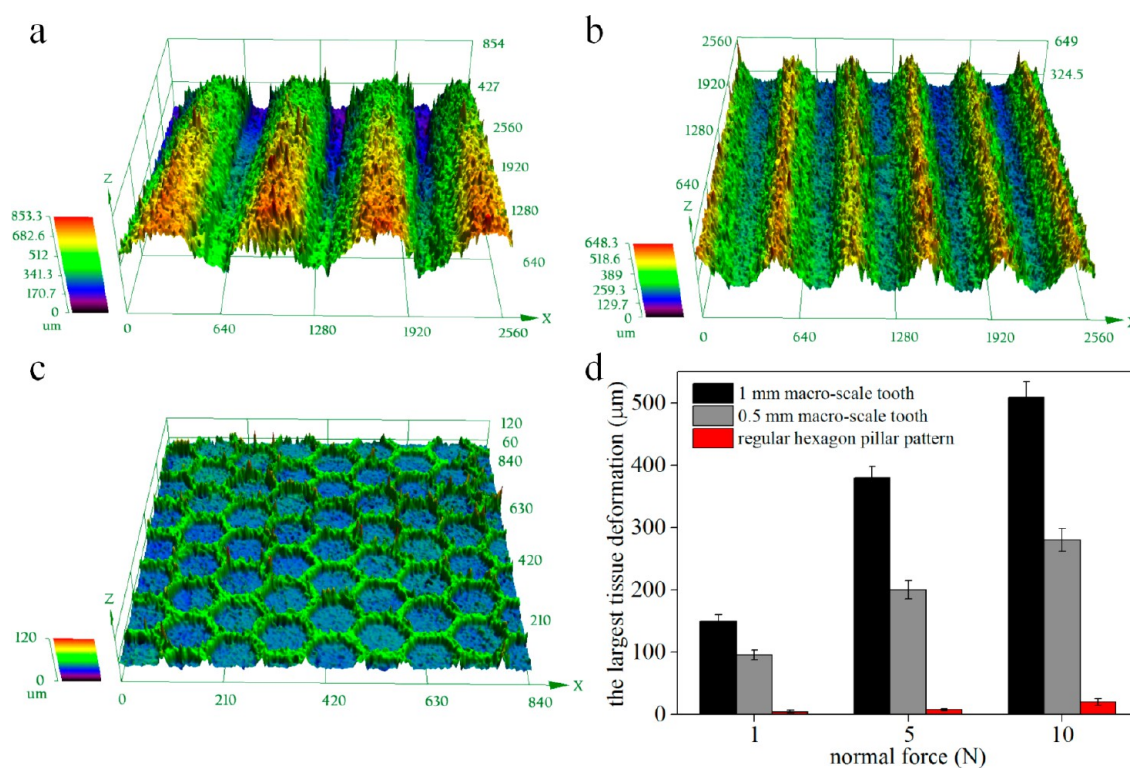


**Figure 11.** (a–c) Deformation of fresh pig liver pressed by 1 mm and 0.5 mm macroscale teeth and hexagonal pillar pattern with a normal force of 10 N. (d) Comparison of the largest tissue deformation induced by 1 mm and 0.5 mm macroscale teeth and hexagonal pillar pattern under normal forces of 1, 5, and 10 N.

measured at one tenth of the deformation induced by 1 mm macroscale teeth (Figure 11d). Tissue deformation will also rise with increases in the normal force. When the normal force reaches 10 N, gaps between the teeth are almost filled with tissue, but the tissue deformation in the hexagonal pillar pattern is only filling the channels, whose depth is  $\sim 30 \mu\text{m}$ . Because the hexagonal pillar pattern can generate strong friction on tissue, less grip force will be needed for grasping, and tissue damage can be prevented. Even if the slipping of tissue occurred on the surface of the surgical grasper, the soft tissue would be less damaged with the hexagonal pillar pattern, because of its smooth structure, whereas the sharp teeth would scratch the tissue and cause some damage.

#### 4. CONCLUSION

The microscale structure characteristics of the tree frog toe pad were observed by SEM, and its structural features were investigated. The anisotropic epithelial cells lead to toe pad friction direction dependence. When comparing the jaw of a modern surgical grasper to micropatterns with hexagonal pillars, rhomboid pillars, triangular pillars, and quadrangular pillars, the hexagonal pillar pattern was found to exhibit a strong and stable friction on soft tissue. Hexagonal pillars with different aspect ratios were compared using the inspiration of irregular hexagon cells on the tree frog toe pads. With a higher aspect ratio, a slimmer hexagonal pillar will exhibit more friction in the corner direction and stronger direction-dependent features. Finally, we compared the tissue damage induced by hexagonal pillar patterns and modern surgical grasper teeth patterns. The hexagonal pillar pattern demonstrates low tissue deformation and results in less tissue damage. Its utility for application in surgical graspers was validated. Using the analysis of epithelial cells on tree frog toe pads and a comparison of different types of micropatterns, the mechanisms for smooth attachment systems have been improved, and these results will help us design more efficient and stronger biomimetic surface patterns.

#### ■ ASSOCIATED CONTENT

##### Supporting Information

Video S1 shows surface sliding with the hexagon corner toward the sliding direction; black parts are ink in the channels. Video S2 shows surface sliding with the hexagon side toward the sliding direction; dark trails on top of the hexagonal pillars show the liquid flow on the top of the hexagonal pillars. The Supporting Information is available free of charge on the ACS Publications website at DOI: 10.1021/acsami.5b03039.

#### ■ AUTHOR INFORMATION

##### Corresponding Authors

\*E-mail: chenhw75@buaa.edu.cn (H. Chen).

\*E-mail: zhangdy@buaa.edu.cn (D. Zhang).

##### Notes

The authors declare no competing financial interest.

#### ■ ACKNOWLEDGMENTS

This work was supported by the NSFC (No. 51175020) and the NSFC Major Program (No. 51290292).

#### ■ REFERENCES

- (1) Peters, J. H.; Gibbons, G.; Innes, J.; Nichols, K.; Roby, S.; Ellison, E. Complications of Laparoscopic Cholecystectomy. *Surgery* **1991**, *110*, 769–778 (discussion on pp 777–778).
- (2) Ponsky, J. L. Complications of Laparoscopic Cholecystectomy. *Am. J. Surg.* **1991**, *161*, 393–395.
- (3) Soper, N. J.; Dunnegan, D. L. Does Intraoperative Gallbladder Perforation Influence the Early Outcome of Laparoscopic Cholecystectomy? *Surg. Laparosc. Endosc. Percutaneous Tech.* **1991**, *1*, 156–161.
- (4) Donohue, J. H.; Farnell, M. B.; Grant, C. S.; van Heerden, J. A.; Wahlstrom, H. E.; Sarr, M. G.; Weaver, A. L.; Ilstrup, D. M. In *Laparoscopic Cholecystectomy: Early Mayo Clinic Experience*; Mayo Clinic Proceedings; Elsevier: Amsterdam, 1992; pp 449–455.
- (5) Johnston, S.; O'Malley, K.; McEntee, G.; Grace, P.; Smyth, E.; Bouchier-Hayes, D. The Need to Retrieve the Dropped Stone During Laparoscopic Cholecystectomy. *Am. J. Surg.* **1994**, *167*, 608–610.
- (6) Chin, P. T.; Boland, S.; Percy, J. P. "Gallstone Hip" and Other Sequelae of Retained Gallstones. *HPB Surg.* **1997**, *10*, 165–168.
- (7) Graham, M. D.; Anderson, P. G.; Toouli, J. Abdominal Wall Sinus: A Late Complication of Gallstone Spillage During Laparoscopic Cholecystectomy. *HPB Surg.* **1997**, *10*, 163–164.
- (8) Patterson, E. J.; Nagy, A. G. Don't Cry over Spilled Stones? Complications of Gallstones Spilled During Laparoscopic Cholecystectomy: Case Report and Literature Review. *Can. J. Surg.* **1997**, *40*, 300–304.
- (9) Schrenk, P.; Woisetschlager, R.; Rieger, R.; Wayand, W. Mechanism, Management, and Prevention of Laparoscopic Bowel Injuries. *Gastrointest. Endosc.* **1996**, *43*, 572–574.
- (10) Bishoff, J. T.; Allaf, M. E.; Kirkels, W.; Moore, R. G.; Kavoussi, L. R.; Schroder, F. Laparoscopic Bowel Injury: Incidence and Clinical Presentation. *J. Urol.* **1999**, *161*, 887–890.
- (11) Dargahi, J.; Parameswaran, M.; Payandeh, S. A Micromachined Piezoelectric Tactile Sensor for an Endoscopic Grasper—Theory, Fabrication and Experiments. *J. Microelectromech. Syst.* **2000**, *9*, 329–335.
- (12) Roan, P. R.; Wright, A. S.; Lendvay, T. S.; Sinanan, M. N.; Hannaford, B. An Instrumented Minimally Invasive Surgical Tool: Design and Calibration. *Appl. Bionics Biomech.* **2011**, *8*, 173–190.
- (13) Vonck, D.; Goossens, R.; Van Eijk, D.; De Hingh, I.; Jakimowicz, J. Vacuum Grasping as a Manipulation Technique for Minimally Invasive Surgery. *Surg. Endosc.* **2010**, *24*, 2418–2423.
- (14) Marucci, D. D.; Cartmill, J. A.; Walsh, W. R.; Martin, C. J. Patterns of Failure at the Instrument–Tissue Interface. *J. Surg. Res.* **2000**, *93*, 16–20.
- (15) Heijnsdijk, E. A. M.; deVisser, H.; Dankelman, J.; Gouma, D. J. Slip and Damage Properties of Jaws of Laparoscopic Graspers. *Surg. Endosc.* **2004**, *18*, 974–979.
- (16) Huber, G.; Mantz, H.; Spolenak, R.; Mecke, K.; Jacobs, K.; Gorb, S. N.; Arzt, E. Evidence for Capillary Contributions to Gecko Adhesion from Single Spatula Nanomechanical Measurements. *Proc. Natl. Acad. Sci. U.S.A.* **2005**, *102*, 16293–16296.
- (17) Sun, W. X.; Neuzil, P.; Kustandi, T. S.; Oh, S.; Samper, V. D. The Nature of the Gecko Lizard Adhesive Force. *Biophys. J.* **2005**, *89*, L14–L17.
- (18) Dirks, J. H.; Federle, W. Fluid-Based Adhesion in Insects—Principles and Challenges. *Soft Matter* **2011**, *7*, 11047–11053.
- (19) Federle, W.; Barnes, W.; Baumgartner, W.; Drechsler, P.; Smith, J. Wet but Not Slippery: Boundary Friction in Tree Frog Adhesive Toe Pads. *J. R. Soc., Interface* **2006**, *3*, 689–697.
- (20) Smith, J. M.; Barnes, W. J. P.; Downie, J. R.; Ruxton, G. D. Structural Correlates of Increased Adhesive Efficiency with Adult Size in the Toe Pads of Hylid Tree Frogs. *J. Comput. Physiol., A* **2006**, *192*, 1193–1204.
- (21) Barnes, W. J. Functional Morphology and Design Constraints of Smooth Adhesive Pads. *MRS Bull.* **2007**, *32*, 479–485.
- (22) Barnes, W. J.; Baum, M.; Peisker, H.; Gorb, S. N. Comparative Cryo-Sem and Afm Studies of Hylid and Rhacophorid Tree Frog Toe Pads. *J. Morphol.* **2013**, *274*, 1384–1396.



(23) Endlein, T.; Barnes, W. J. P.; Samuel, D. S.; Crawford, N. A.; Biaw, A. B.; Grafe, U. Sticking under Wet Conditions: The Remarkable Attachment Abilities of the Torrent Frog, *Staurois Guttatus*. *PLoS One* **2013**, *8*, e73810.

(24) Shahsavan, H.; Zhao, B. X. Bioinspired Functionally Graded Adhesive Materials: Synergetic Interplay of Top Viscous-Elastic Layers with Base Micropillars. *Macromolecules* **2014**, *47*, 353–364.

(25) Roshan, R.; Jayne, D.; Liskiewicz, T.; Taylor, G.; Gaskell, P.; Chen, L.; Montellano-Lopez, A.; Morina, A.; Neville, A. Effect of Tribological Factors on Wet Adhesion of a Microstructured Surface to Peritoneal Tissue. *Acta Biomater.* **2011**, *7*, 4007–4017.

(26) del Campo, A.; Greiner, C. Su-8: A Photoresist for High-Aspect-Ratio and 3d Submicron Lithography. *J. Micromech. Microeng.* **2007**, *17*, R81–R95.

(27) Rosen, J.; Brown, J. D.; De, S.; Sinanan, M.; Hannaford, B. Biomechanical Properties of Abdominal Organs *In Vivo* and *Postmortem* under Compression Loads. *J. Biomech. Eng.—Trans. ASME* **2008**, *130*, 021020–021020.

(28) Seo, S.; Lee, J.; Kim, K.-S.; Ko, K. H.; Lee, J. H.; Lee, J. Anisotropic Adhesion of Micropillars with Spatula Pads. *ACS Appl. Mater. Interfaces* **2014**, *6*, 1345–1350.

(29) Tsipenyuk, A.; Varenberg, M. Use of Biomimetic Hexagonal Surface Texture in Friction against Lubricated Skin. *J. R. Soc. Interface* **2014**, *11*, 20140113.

(30) Iturri, J.; Xue, L. J.; Kappl, M.; Garcia-Fernandez, L.; Barnes, W. J. P.; Butt, H. J.; del Campo, A. Torrent Frog-Inspired Adhesives: Attachment to Flooded Surfaces. *Adv. Funct. Mater.* **2015**, *25*, 1499–1505.